JOURNAL OF Materials CHEMISTRY

Phase transitions in $Ca_{1-x}Sr_xTiO_3$ perovskites: effects of composition and temperature

Shan Qin,†[a] Ana I. Becerro,*[a] Friedrich Seifert,[a] Joachim Gottsmann[a] and Jianzhong Jiang[b]

[a]*Bayerisches Geoinstitut, Universität Bayreuth, D-95440 Bayreuth, Germany. E-mail: Ana-Isabel.Becerro@uni-bayreuth.de*
[b]*Department of Physics, Technical University of Denmark, DK-2800 Lyngby, Denmark*

Received 24th January 2000, Accepted 17th April 2000
Published on the Web 21st June 2000

The crystal structures of $Ca_{0.6}Sr_{0.4}TiO_3$ and $Ca_{0.8}Sr_{0.2}TiO_3$ perovskites have been studied at high temperatures by X-ray powder diffraction. The most likely sequence of phase transitions with increasing temperature in $Ca_{0.6}Sr_{0.4}TiO_3$ is the same as that shown by the system $CaTiO_3$–$SrTiO_3$ with increasing Sr content at room temperature. This sequence is: orthorhombic *Pbnm*, orthorhombic *Bmmb*, tetragonal *I*4/*mcm* and cubic $Pm\bar{3}m$. The second orthorhombic phase could not be determined in $Ca_{0.8}Sr_{0.2}TiO_3$, either due to the poorer resolution of the diffractometer employed or because the *Bmmb* phase might not have a stability field at this composition. The transition temperatures decrease on going from $Ca_{0.8}Sr_{0.2}TiO_3$ to $Ca_{0.6}Sr_{0.4}TiO_3$. Calorimetric measurements on 12 samples spanning the system $CaTiO_3$–$SrTiO_3$ then allow one to draw, in combination with the RT XRD data, the temperature *vs.* composition phase diagram. Phase boundaries show a linear shift toward lower Sr content with the increase of temperature, implying a negligible plateau effect near the $CaTiO_3$ composition, but quantum saturation occurs at low temperatures near the $SrTiO_3$ composition.

Introduction

Perovskite type oxides of general formula ABO_3[1] are important in material sciences, physics and earth sciences, *e.g.* for their electric properties,[2] their ability to immobilise high-level radioactive waste[3] and as the dominant mineral in the Earth's lower mantle. They are also well-known for their phase transitions, which may strongly affect their physical and chemical properties. Especially the ternary system formed by the compounds barium titanate, calcium titanate and strontium titanate is of great interest in the field of dielectrics. Both the $BaTiO_3$–$CaTiO_3$ and the $BaTiO_3$–$SrTiO_3$ systems have been studied extensively (see refs. 4,5 and references therein). Several authors have also studied the system $CaTiO_3$–$SrTiO_3$. At room temperature, the $CaTiO_3$ end member exhibits the orthorhombic space group *Pbnm*—another setting of the conventional *Pnma*[6]—while the $SrTiO_3$ end member is cubic with space group $Pm\bar{3}m$.[7] However, the structures and phase boundaries in the intermediate phases of this system ($Ca_{1-x}Sr_xTiO_3$) have been controversial.[4,8–14] Recently Ball *et al.*[12] reported a sequence of phase transitions with increasing Sr content from orthorhombic *Pnma* ($0 \leqslant x \leqslant 0.4$), orthorhombic *Bmmb* ($0.45 \leqslant x \leqslant 0.6$), tetragonal *I*4/*mcm* ($0.65 \leqslant x \leqslant 0.9$) to cubic $Pm\bar{3}m$ ($x \geqslant 0.95$). However, Ranjan *et al.*[13] claimed that the structure remains orthorhombic to $x \leqslant 0.88$.

In this system phase transitions as a function of temperature have only been determined over a sufficient temperature range for the $CaTiO_3$ end member: Redfern,[15] by *in-situ* X-ray diffraction, located a *Pbnm* to *I*4/*mcm* transition in the range 1100–1150 °C, followed by transformation to the $Pm\bar{3}m$ aristotype at around 1250 °C. More recently, Kennedy *et al.*,[16] based on high temperature neutron diffraction measurements, suggested an additional phase transition from the room temperature *Pbnm* to another orthorhombic structure *Cmcm* (the conventional setting for *Bmmb*) at 1107 °C, *i.e.* the same sequence of phase transitions as in the system $CaTiO_3$–$SrTiO_3$ with increasing Sr content at room temperature found by Ball *et al.*[12] Temperature–composition (*T*–*X*) information on the other members of the system is still very scarce, because Ball *et al.*[12] were limited to 500 °C, and Ranjan and Pandey[14] only studied compositions very close to $SrTiO_3$ ($x \geqslant 0.79$).

In this study we analyse, by means of X-ray powder diffraction, the structures of two particularly relevant compositions ($Ca_{0.6}Sr_{0.4}TiO_3$ and $Ca_{0.8}Sr_{0.2}TiO_3$) with increasing temperature, thus determining transition temperatures. In addition, we confirm the sequence of phase transitions at room temperature as a function of composition in the system $CaTiO_3$–$SrTiO_3$. Finally, calorimetric data are used, in combination with the high temperature XRD data, to derive the temperature–composition phase diagram of the binary system for temperatures above ambient.

Experimental

15 powder samples of the $Ca_{1-x}Sr_xTiO_3$ system with nominal compositions $x = 0$ to 1 were synthesized by drying $CaCO_3$ (Chempur, 99.9%) and $SrCO_3$ (Aldrich, 99.999%) at 500 °C and TiO_2 (Aldrich, 99.9%) at 1000 °C for 3 hours. Mixtures of stoichiometric amounts were heated to 1300 °C at a rate of 20 °C h^{-1} and kept at that temperature for 4 hours. After grinding in an agate mortar, the samples were fired in air at 1600 °C for 48 hours with periodic regrinding, and finally rapidly cooled. The materials were then analysed with a Cameca SX-50 electron microprobe operating at an accelerating voltage of 15 kV and a using beam current of 15 nA. A range of synthetic materials was used for standardisation and all data were reduced using the PAP correction routine. The microprobe analysis showed the materials to be close to the nominal composition and homogeneous at the 1% level: columns 1 and 2 in Table 1 show the agreement between the nominal and real compositions.

The room temperature study of the samples in the system $CaTiO_3$–$SrTiO_3$ was accomplished using X-ray powder diffraction in a Siemens D-5000 diffractometer with Cu $K\alpha_{1,2}$ radiation. Data were recorded between 20° and 130° 2θ with

†Present address: Department of Geology, Peking University, Beijing 100871, China.

Table 1 Microprobe analysis, cell parameters, cell volume and space groups of $Ca_{1-x}Sr_xTiO_3$ ($0 \leqslant x \leqslant 1$) at RT. The numbers in parentheses are the estimated standard deviations in units of the last digit(s)

Nominal x	Sr/(Sr+Ca)	a/Å	b/Å	c/Å	Cell volume/Å^3	Space group
0.00	0.000 (0)	5.37980(7)	5.44210(8)	7.64036(10)	223.690(6)	*Pbnm*
0.05	0.047(1)	5.39145(10)	5.44427(10)	7.65289(15)	224.632(8)	*Pbnm*
0.10	0.095(2)	5.40192 (12)	5.44600(11)	7.66292(17)	225.434(8)	*Pbnm*
0.15	0.143(3)	5.41190(12)	5.44851(11)	7.67345(17)	226.265(8)	*Pbnm*
0.20	0.192(10)	5.4228(2)	5.4505(1)	7.6842(2)	227.075(6)	*Pbnm*
0.30	0.301(9)	5.4426(3)	5.4581(2)	7.7041(4)	228.860(12)	*Pbnm*
0.40	0.393(10)	5.4562(2)	5.4615(2)	7.7181(2)	229.990(6)	*Pbnm*
0.50	0.494(7)	7.7413(8)	7.7375(7)	7.7396(11)	463.593(12)	*Bmmb*
0.55	0.545(7)	7.7426(3)	7.7492(8)	7.7508(7)	465.040(12)	*Bmmb*
0.60	0.593(7)	7.7485(3)	7.7582(12)	7.7571(13)	466.317(10)	*Bmmb*
0.70	0.699(6)	5.48545(5)		7.79243(10)	234.476(5)	*I*4/*mcm*
0.80	0.793(10)	5.49722(8)		7.80109(18)	235.745(8)	*I*4/*mcm*
0.85	0.844(5)	5.50661(6)		7.80331(15)	236.618(7)	*I*4/*mcm*
0.90	0.905(15)	5.51326(7)		7.80184(19)	237.145(4)	*I*4/*mcm*
1.00	0.999(7)	3.90479(1)			59.538(0)	$Pm\bar{3}m$

steps of 0.02° and counting time of 10 s per step. Silicon was applied as an internal standard.

Members with $x = 0.40$ and $x = 0.20$ were selected for the high temperature study because they should undergo all the different phase transitions in an appropriate range of temperatures.[12] The patterns were collected from room temperature up to 1150 °C with different temperature steps for each sample. Two different high temperature diffractometers were used: the XRD measurements on the $x = 0.40$ sample were recorded in the high temperature diffractometer described by Salje *et al.*[17] which uses a curved 120° position-sensitive detector. The sample with $x = 0.20$ was analysed in a STOE reflection diffractometer equipped with an oven up to 1150 °C and the temperature stability was maintained (±2 °C) by a Eurotherm controller connected by a Pt/PtRh thermocouple welded onto the Pt heater. Both diffractometers use Cu Kα radiation and powdered α-Al_2O_3 was mixed with the sample to act as an internal standard.

Data were analysed using the Rietveld method with the GSAS software.[18] The refined parameters in the RT XRD study were background coefficients, histogram scale factors, lattice parameters, linewidths, phase fractions and atomic positions. In the high temperature study no realistic atomic positions could be refined with acceptable standard deviations and atomic positions of oxygen atoms were therefore fixed at the values given by the room temperature study for the respective space groups.

The specific heat capacities were determined using a differential scanning calorimeter DSC 111 Setaram for samples with $0.30 \leqslant x \leqslant 0.80$. Two other calorimeters—STA 449 Netzsch and L81 Linseis—had to be used for samples with $x \leqslant 0.30$ due to the higher transition temperatures shown by these samples. The powdered samples were placed in platinum crucibles in the two first machines and in Al_2O_3 crucibles in the third one, and heated at constant heating rates of 5 K min^{-1} in the DSC 111 and of 10 K min^{-1} in the two other calorimeters. The DSC111 calorimeter is calibrated against the heat capacity of a single-crystal of sapphire with matching geometries. Heat capacity data of sapphire are taken from Robie *et al.*[19] The accuracy of temperature is ±3 K, derived from calibration against the phase transition temperatures of KCl, Ag_2SO_4, SiO_2, K_2SO_4, K_2CrO_4 and $BaCO_3$. To further account for the effect of heating rate on the apparent transition temperatures, the α–β phase transition of quartz (573 °C) was used for calibration. The transition temperatures given for samples with $x = 0.30$ are the average from the three calorimeters and those for $x \leqslant 0.20$, the average data obtained from STA 449 Netzsch and L81 Linseis machines.

Results

A: Effects of composition

The ideal perovskite structure has an ABO_3 stoichiometry and the aristotype has the cubic space group $Pm\bar{3}m$. Distortions from the ideal cubic structure are commonly due to tilting of the octahedra and can be realised by tilting essentially rigid MO_6 octahedra while maintaining their corner-sharing connectivity. The transition from *Pbnm* ($a^+b^-b^-$) to *Bmmb* ($a^0b^+c^-$) involves the disappearance of one of the three octahedral rotations, while in transforming *Pbnm* to *I*4/*mcm* ($a^0a^0c^-$) two of the tilts are removed. The tilts break the $Pm\bar{3}m$ symmetry and produce a series of weak superlattice reflections in the diffraction pattern that are diagnostic of the space group of the phase.[20]

Fig. 1 exhibits the room temperature XRD diagrams between 36° and 42° 2θ of selected $Ca_{1-x}Sr_xTiO_3$ phases, with the critical reflections for the expected space groups indicated. As a function of composition some peaks or groups of peaks (*e.g.* $(120, 210)_{Pbnm}$) disappear with higher x and other groups of peaks merge into single peaks. For the latter it is important to note that the patterns also contain Cu $K_{\alpha 2}$ contributions with the consequent splitting of each line into two. The splitting of 022 and 202 reflections of the

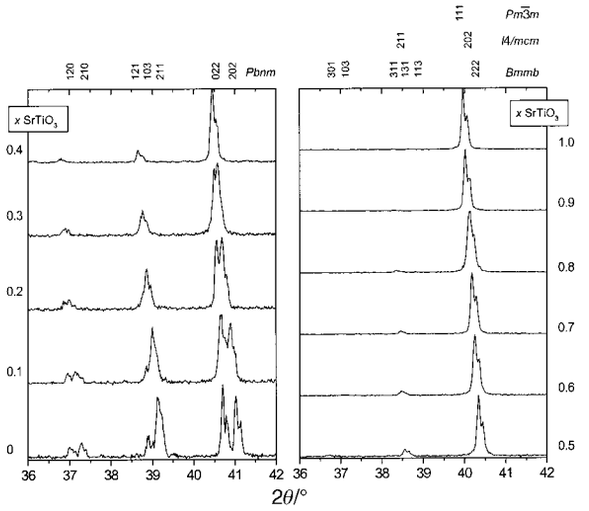

Fig. 1 Portion of XRD ($\lambda = 1.5406$ Å) patterns of $Ca_{1-x}Sr_xTiO_3$ ($0 \leqslant x \leqslant 1$), showing the composition dependence of the superlattice reflections. Critical reflections for the expected space groups are indicated on top of the diagram.

orthorhombic *Pbnm* phase (at around 41° 2θ) is clear at $0 \leqslant x \leqslant 0.3$. At $x = 0.40$ the single peak is broader than at higher Sr contents, indicating that it is still composed of two lines. From the superlattice reflections and peak splitting, supported by structural refinements, we conclude that the structures with $0 \leqslant x \leqslant 0.40$ are *Pbnm*. The lattice parameters (reduced to those of a pseudocubic sub-cell) obtained from the refinement of these structures and of the rest of the solid solution (which will be commented upon below) are shown in Fig. 2 and Table 1. The lattice parameters of the *Pbnm* phase converge near $x = 0.4$, which indicates either a crossover or a transition to a new symmetry.

At $x = 0.50$ there is still some intensity left at $\approx 37.8°$ 2θ characteristic of orthorhombic distortion. At $0.55 \leqslant x \leqslant 0.90$, lines 120 and 210 of the *Pbnm* phase are absent or too weak to be detected (Fig. 1) whereas diffraction peaks of decreasing intensity remain just below 39° 2θ. These observations might suggest that the structures in this compositional range are tetragonal *I4/mcm*. However, an XRD study by Ball *et al.*[12] using synchrotron radiation allowed them to register very weak superlattice reflections in samples with $0.50 \leqslant x \leqslant 0.60$ which indicate that the lattice is not body-centred. Likely alternatives are Glazer's tilt systems[21] No 17 and 18, both of which give rise to an orthorhombic structure with space group *Bmmb*. Neither of these tilt systems will account for all of the superlattice reflections observed by Ball *et al.*[12] but the space group allows for A-cation displacements and for distortion of the octahedra that will account for the extra lines. The other alternative would be the persistence of the *Pbnm* space group beyond $x = 0.40$. The diffractometer employed in the present study did not allow us to register these weak superlattice reflections; however the refinement on the basis of space group *I4/mcm* for $x \geqslant 0.50$ yielded a clear discontinuity in the lattice constants near $x = 0.65$ that suggests a phase boundary. We then refined the diagrams of the compositions $0.50 \leqslant x \leqslant 0.60$ on the basis of the space group *Bmmb* obtaining χ^2 values significantly lower than for *I4/mcm* and slightly lower than for *Pbnm*. The linewidth had to be fixed, probably because of the similarity of the length of the axes. We therefore conclude that the structures in this compositional range might be *Bmmb* although we cannot exclude *Pbnm* in the entire region $0 \leqslant x \leqslant 0.60$. The lack of the $(301, 103)_{Bmmb}$ reflections in these patterns (Fig. 1) is explained by their low intensities (less than 1% of the intensity of the $(222)_{Bmmb}$ reflection according to the refinements). Finally, the extrapolation of the reduced cell parameters for *I4/mcm* in the range $0.70 \leqslant x \leqslant 0.90$ suggests that the cubic phase boundary is near $x = 0.92$, in agreement with the cubic $Pm\bar{3}m$ structure of the Sr-rich end member. Cell volumes (*cf.* Table 1) vary nearly linearly across the entire join.

We therefore conclude that, at room temperature, the most likely sequence of phases in $Ca_{1-x}Sr_xTiO_3$ system is *Pbnm*, *Bmmb*, *I4/mcm* and $Pm\bar{3}m$ with increasing strontium content, in good agreement with Ball *et al.*[12] The phase boundaries are located at $x = 0.45(5)$ for *Pbnm–Bmmb*, 0.65(5) for *Bmmb–I4/mcm* and 0.92(2) for *I4/mcm–*$Pm\bar{3}m$.

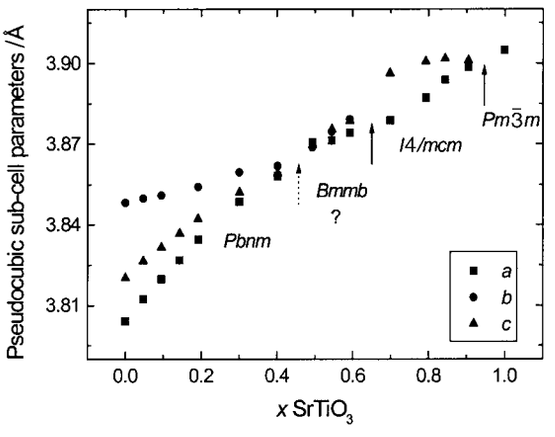

Fig. 2 Pseudocubic sub-cell parameters plotted as a function of x in the $Ca_{1-x}Sr_xTiO_3$ system at room temperature. $a = a_o/\sqrt{2}$, $b = b_o/\sqrt{2}$ and $c = c_o/2$ where a_o, b_o and c_o are the lattice parameters of the unit cell.

B: Effects of temperature

Analysis of X-ray powder diffraction data (at temperatures up to 1150 °C) for $Ca_{0.6}Sr_{0.4}TiO_3$ and $Ca_{0.8}Sr_{0.2}TiO_3$ perovskites followed the same strategy of examination of weak superlattice peaks and extrapolation of lattice constants as explained above.

The structure of $Ca_{0.6}Sr_{0.4}TiO_3$ between room temperature and 350 °C was refined in the *Pbnm* space group. Splitting of lines is already weak at room temperature (*cf.* Fig. 1), and further decreases with temperature. The $222_{Pm\bar{3}m}$ peak near 87° 2θ proved to be diagnostic: taking the overall linewidth of the patterns as an additional guide, it had to be fitted to two peaks up to 350 °C, whereas at 400 °C it seems to be a single peak. Patterns recorded from 400 °C to 700 °C are compatible with space group *I4/mcm* but, similar to the room temperature behaviour with increasing Sr content, the cell parameters show a discontinuity between 500 °C and 550 °C, suggesting the presence of a phase boundary. The structures from 400 °C to 500 °C were then refined in both orthorhombic *Bmmb* and *Pbnm*, and the values of χ^2 decreased significantly compared to those obtained in *I4/mcm*. χ^2 values obtained after refining in *Bmmb* were slightly lower than for *Pbnm* and we therefore conclude that *Bmmb* might be the relevant space group for $Ca_{0.6}Sr_{0.4}TiO_3$ between 400 °C and 500 °C although we can not exclude *Pbnm* in the entire temperature range (RT–500 °C). From 550 °C to 750 °C the superlattice reflections indicate that the structure is tetragonal with space group *I4/mcm* while for temperatures $\geqslant$850 °C the diagrams are compatible with cubic symmetry. The XRD pattern at 800 °C only shows cubic reflections but the linewidth obtained in the refinement is still compatible with tetragonal symmetry. These results therefore suggest that the transition temperature from tetragonal to cubic symmetry is located at around 800 °C. The variation with temperature of the cell parameters is shown in Table 2 and plotted (reduced to those of a pseudocubic subcell) in Fig. 3. No cell parameter is given for 800 °C, due to the aforementioned uncertainty. Some of the Rietveld fits are shown in Fig. 4. The mean thermal expansion coefficients for cell edge lengths and volume in every phase are shown in Table 3.

The transition temperatures in $Ca_{0.6}Sr_{0.4}TiO_3$ perovskite are, therefore, 525(25) °C for orthorhombic (*Pbnm* or *Bmmb*)–*I4/mcm*, and 800(50) °C for *I4/mcm–*$Pm\bar{3}m$. If *Bmmb* space group had a stability field between 400 and 500 °C, the *Pbnm–Bmmb* boundary would be at *ca.* 375 °C.

We have also registered the XRD patterns for $Ca_{0.8}Sr_{0.2}TiO_3$ at temperatures near the expected transitions and used the superlattice reflections to deduce the space group at each temperature. In this case, the poorer resolution of the diffractometer employed together with the similarity of the axis length in the space group *Bmmb* did not allow us to refine the corresponding diagrams on the basis of *Bmmb*. Similar to the case of $x = 0.4$ uncertainty remains about the space group (*Pbnm* or *Bmmb*) close to the transition to tetragonal. The transition temperatures found for $x = 0.20$ are 875(25) °C for orthorhombic (*Pbnm* or *Bmmb*)–*I4/mcm* and 1100(50) °C for *I4/mcm–*$Pm\bar{3}m$.

Therefore, the sequence of symmetry changes with increasing Sr content at RT in the system $CaTiO_3$–$SrTiO_3$ and with increasing temperature in intermediate compositions of the system is the same: orthorhombic–tetragonal–cubic. This sequence can be explained, in both cases, in the same terms of tolerance factor because increasing the size of the atom in the A site—$r(Sr^{2+}) > r(Ca^{2+})$—has the same effect as increasing

Table 2 Cell parameters and space groups for $Ca_{0.6}Sr_{0.4}TiO_3$ as a function of temperature. The numbers in parentheses are the estimated standard deviations in units of the last digit(s)

T/°C	a/Å	b/Å	c/Å	V/Å^3	Space group
25	5.4517(8)	5.4615(9)	7.7089(13)	229.53(3)	*Pbnm*
150	5.4631(4)	5.4745(5)	7.3238(8)	231.01(2)	*Pbnm*
350	5.4774(4)	5.4912(4)	7.7428(6)	232.88(2)	*Pbnm*
400	7.7544(10)	7.7602(7)	7.7697(7)	467.55(5)	*Bmmb*
450	7.7575(9)	7.7648(12)	7.7744(7)	468.29(5)	*Bmmb*
500	7.7683(25)	7.7658(22)	7.7826(6)	469.50(2)	*Bmmb*
550	5.4916(2)		7.7905(4)	234.95(1)	*I*4/*mcm*
600	5.4959(2)		7.7988(5)	235.56(1)	*I*4/*mcm*
650	5.4986(2)		7.8013(5)	235.87(1)	*I*4/*mcm*
700	5.5041(2)		7.8069(6)	236.52(1)	*I*4/*mcm*
750	5.5077(2)		7.8089(6)	236.88(1)	*I*4/*mcm*
850	3.9056(1)			59.57(1)	$Pm\bar{3}m$
900	3.9069(1)			59.64(1)	$Pm\bar{3}m$
950	3.9112(1)			59.83(1)	$Pm\bar{3}m$
1000	3.9131(1)			59.92(1)	$Pm\bar{3}m$

temperature (increase of the thermal vibration of the atoms).[22] Higher resolution experiment are still necessary to define the stability field of the second orthorhombic phase (*Bmmb*).

C: Calorimetric study

In order to obtain transition temperatures for all the compositions we have carried out calorimetric measurements. The heat capacity curves of samples with $0 \leqslant x \leqslant 0.65$ are very similar to each other and exhibit two peaks with peak temperatures shifting to lower values with increasing Sr content. Fig. 5 shows, as an example, the heat capacity curve of $Ca_{0.5}Sr_{0.5}TiO_3$ perovskite. The first peak is associated with a usual λ-type curve where the heat capacity decrease after the transition is sharp. In contrast, the second transition shows a broad peak with a large heat capacity tail towards high temperatures. The peak temperatures of our heat capacity curve for $Ca_{0.6}Sr_{0.4}TiO_3$ (536 °C and 803 °C) are in good agreement with the temperatures for the orthorhombic (*Pbnm* or *Bmmb*)–*I*4/*mcm* and *I*4/*mcm*–$Pm\bar{3}m$ transitions obtained by means of the high temperature XRD study above. Likewise, the DSC curve for $Ca_{0.8}Sr_{0.2}TiO_3$ shows a clear peak at 889.3 °C that agrees with the temperature for the orthorhombic–*I*4/*mcm* transition found by means of high temperature XRD. The transition to cubic symmetry is not clear in the DSC curve for this composition, but in the temperature region where the XRD study locates it, we find a tiny peak that could well be due to that transition. Therefore we conclude that for every composition with $0 \leqslant x \leqslant 0.65$, the λ-type peak results from the orthorhombic (*Pbnm* or *Bmmb*)–*I*4/*mcm* transition and the broader peak located at higher temperature, from the *I*4/*mcm*–$Pm\bar{3}m$ transition. The transition between the two orthorhombic space groups (*Pbnm*–*Bmmb*), on the other hand, is not visible in the DSC data (for possible reasons see below).

Finally, samples with $x = 0.70$ and $x = 0.793$ only show one peak corresponding to the tetragonal to cubic transition because for these compositions the orthorhombic–tetragonal transition occurs at temperatures below zero which are not in the range of the calorimeters employed. Table 4 shows the transition temperatures for all the compositions.

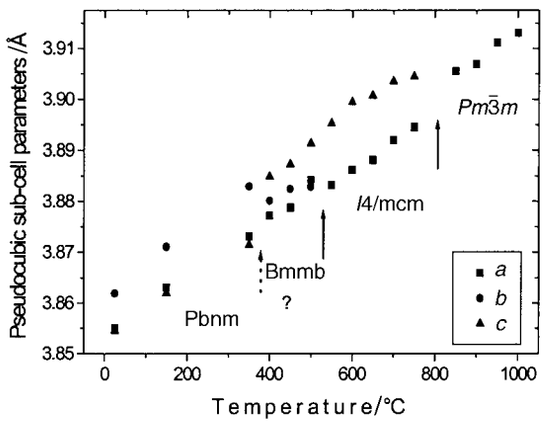

Fig. 3 Pseudocubic sub-cell parameters for $Ca_{0.6}Sr_{0.4}TiO_3$ as a function of temperature. $a = a_o/\sqrt{2}$, $b = b_o/\sqrt{2}$ and $c = c_o/2$ where a_o, b_o and c_o are the lattice parameters of the unit cell.

D: Temperature *vs.* composition diagram

Transition temperatures in Table 4 have been used to build the phase diagram shown in Fig. 6. Both orthorhombic–tetragonal

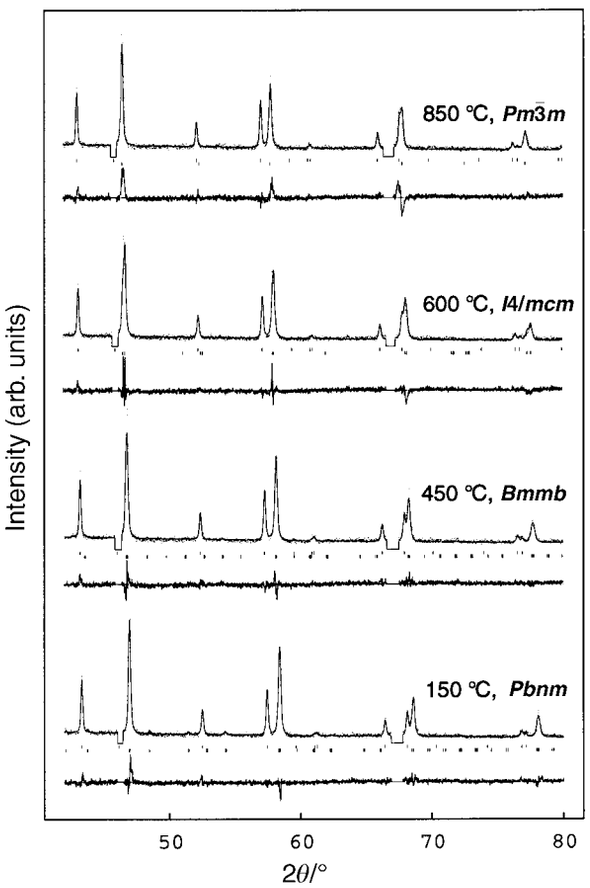

Fig. 4 Selected XRD data ($\lambda = 1.5406$ Å) and calculated patterns for $Ca_{0.6}Sr_{0.4}TiO_3$ at different temperatures. The experimental data are shown as dots, the calculated fits and difference curves as solid lines. Tick marks (upper row for internal standard Al_2O_3) indicate the calculated reflection positions. Flat regions correspond to Pt (due to the sample holder) which was excluded for the refinement.

Table 3 Thermal expansion coefficients for $Ca_{0.6}Sr_{0.4}TiO_3$ in different phases

Temperature ranges/°C	α_a (Unit × 10^{-5}/°C)	α_b	α_c	α_V	Space group
25–350	1.45	1.67	1.35	4.49	*Pbnm*
400–500	1.79	0.72	1.60	4.17	*Bmmb*
550–750	1.47		1.18	4.11	*I4/mcm*
850–1000	1.28			3.92	*Pm$\bar{3}$m*

(*I4/mcm*) and *I4/mcm*–cubic (*Pm$\bar{3}$m*) phase boundaries shift linearly towards higher temperature values with decreasing Sr content. Transition temperatures reported by Ranjan and Pandey[14] for the tetragonal to cubic transition at $x \geqslant 0.79$ perfectly fit into the line that defines the *I4/mcm–Pm$\bar{3}$m* phase boundary.

The solid lines in the diagram are linear fits of the DSC data corresponding to the orthorhombic–*I4/mcm* and *I4/mcm–Pm$\bar{3}$m* transitions for $x \geqslant 0.05$. It should be noted that the *Bmmb–I4/mcm* and *I4/mcm–Pm$\bar{3}$m* phase transitions in $CaTiO_3$ perovskite lie very close to or in the linear trends in the *T–X* diagram.

No boundary can be depicted between the *Pbnm* and *Bmmb* space groups from the DSC or XRD data. In principle, the RT XRD data point ($x = 0.45(5)$, Fig. 2) and the transition temperature for $CaTiO_3$ (1107 °C[16]) should define a reliable phase boundary given the linearity of the two other transitions. However, our high temperature XRD study does not allow us to definitively confirm the stability field of the second orthorhombic phase and for the time being it is preferable to leave this as an open question.

Discussion

The phase relations and symmetry changes described above form an internally-consistent data set. It is in excellent agreement with respect to the composition-dependent symmetry changes at room temperature as reported by Ball *et al.*[12] The symmetry data at room temperature reported here are, however, at variance with those given by Ranjan *et al.*[13] These authors claim that compositions with $x \leqslant 0.88$ are all orthorhombic. They base this conclusion on the study of superlattice reflections and their relationship with in-phase (+) and *anti*-phase (−) tilting. However, we disagree with them on the following points: They observe that some of the superlattice reflections which are present in the neutron diffraction pattern for $CaTiO_3$ are absent in the pattern for $x = 0.50$; this might be the first indication of a symmetry change from $x = 0$ (*Pbnm*) to $x = 0.50$ (*Bmmb*) as Ball *et al.*[12] and our study show. On the other hand, Ranjan *et al.*[13] report that the remaining superlattice peaks in $x = 0.50$ indicate the presence of − and + tilts and they then carry out the refinement assuming the *Pbnm* space group ($a^-a^-c^+$). However, they do not take into account the *Bmmb* space group which also accounts for both types of tilting ($a^0b^+c^-$). In addition, some of the superlattice reflections are absent in the diffractograms for $x = 0.75$ and $x = 0.88$ in comparison with $x = 0.50$, which is also in agreement with our study where $x = 0.75$ and $x = 0.88$ are tetragonal *I4/mcm*. They propose, as a possible reason for this fact, the absence of the + tilt and suggest a new space group *Ibmm* ($a^-a^-c^0$). However, they do not consider the space group *I4/mcm* that also lacks the + tilt ($a^0a^0c^-$).

The sequence of space groups as a function of temperature for all compositions studied is consistent with that found for $CaTiO_3$,[16] $SrZrO_3$[23–25] and $CaGeO_3$[26] perovskites. The linear *T–X* relationships observed for the orthorhombic–*I4/mcm* and *I4/mcm–Pm$\bar{3}$m* transitions also give support to transformation temperatures in $CaTiO_3$ reported by Kennedy *et al.*:[16] for these

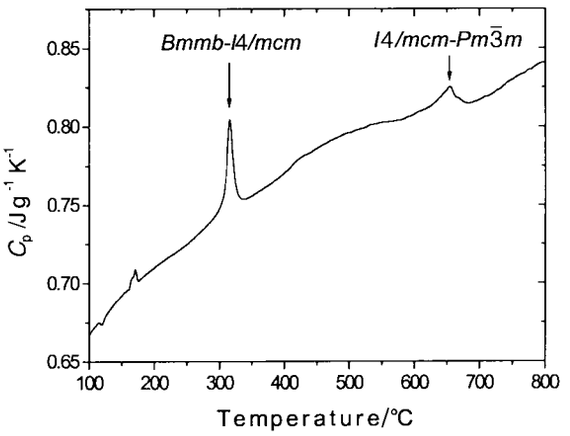

Fig. 5 Heat capacity curve of the $Ca_{0.5}Sr_{0.5}TiO_3$ perovskite. The peaks at around 115 °C and 170 °C are technical artifacts.

two transitions, we find 1242 °C and 1348 °C, respectively (*cf.* Table 4), to be compared to 1227 °C (*Bmmb–I4/mcm*) and 1310 °C (*I4/mcm–Pm$\bar{3}$m*) given by Kennedy *et al.*[16] These temperatures are markedly higher than those given by Redfern[15] for the *Pbnm–I4/mcm* transition (1100–1150 °C) and the *I4/mcm–Pm$\bar{3}$m* transition (*ca.* 1250 °C) in $CaTiO_3$.

In this context, the calorimetric measurements by Guyot *et al.*[27] on $CaTiO_3$ and their interpretation (also followed by Kennedy *et al.*[16]) deserve an additional comment: Guyot *et al.* found two peaks in $CaTiO_3$ (at 1111 °C and 1247 °C) with the same shape characteristics as observed here for the orthorhombic–*I4/mcm* and *I4/mcm–Pm$\bar{3}$m* phase transitions. They associate the first peak, by analogy with the phase transitions for $CaGeO_3$ observed by means of XRD by Liu *et al.*,[26] with the *Pbnm* to *Bmmb* transition while the second one would result from the overlapping of two transitions: *Bmmb–I4/mcm* and *I4/mcm–Pm$\bar{3}$m*. Two observations contradict this assignment. Firstly, the heat capacity curve obtained by Liu *et al.*[26] for $CaGeO_3$ does not show any evidence for either an isothermal absorption of heat or a discontinuity, maximum or lambda anomaly in C_p anywhere in the range of temperature where their XRD study locates the *Pbnm* to *Bmmb* transition. Moreover, according to the accuracy of their calorimetric data they conclude that the enthalpy associated with the transition is very small (probably less than 50 J mol^{-1}, consistent with our observations in $CaTiO_3$–$SrTiO_3$ perovskites). On the other hand, Guyot *et al.*[27] report an enthalpy of about 1 KJ mol^{-1} for the heat capacity anomaly in $CaTiO_3$ at 1111 °C which they

Table 4 Transition temperatures obtained from DSC measurements. DSC curves of $x = 0.095$, $x = 0.192$ and $x = 0.301$ showed extremely broad peaks for the second anomaly that did not allow us to determine an accurate temperature for the *I4/mcm–Pm$\bar{3}$m* transition. The transition temperatures for orthorhombic–*I4/mcm* in $x \geqslant 0.699$ and for *I4/mcm–Pm$\bar{3}$m* in $x > 0.793$ are below the working temperature of our machines (nd = not detected)

x $SrTiO_3$	Transition temperature/°C	
	(*Bmmb* or *Pbnm*)–*I4/mcm*	*I4/mcm–Pm$\bar{3}$m*
0.000	1242	1348.2
0.047	1163.7	1284.5
0.095	1075.2	nd
0.143	991.4	1134
0.192	889.3	nd
0.301	695.3	nd
0.393	536.2	802.7
0.494	314.4	649.6
0.545	208.0	582.0
0.593	114.5	525.2
0.699	nd	384.0
0.793	nd	238.8

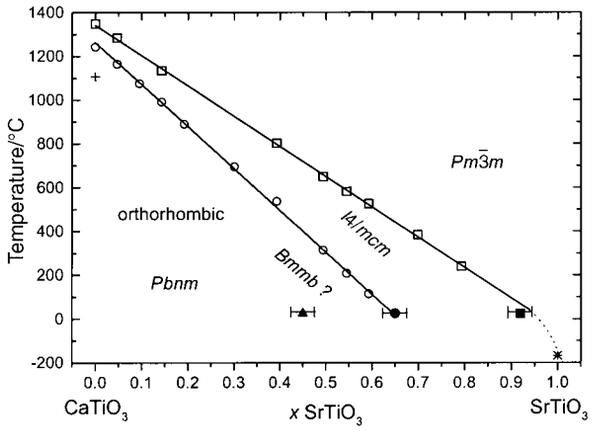

Fig. 6 Variation of phase boundaries, with composition and temperature, in the $Ca_{1-x}Sr_xTiO_3$ system. Open symbols: DSC data, solid symbols: RT XRD data, asterisk: Hayward and Salje,[30] cross: Kennedy *et al.*[16] The existence of a second orthorhombic field (*Bmmb*) close to the transition to tetragonal symmetry remains open.

assign to a *Pbnm–Bmmb* transition. This enthalpy value is, according to our data (not shown here because a quantitative study of the DSC curves will be published separately), rather a characteristic value for the orthorhombic–*I4/mcm* transition in this composition. We conclude that Guyot *et al.*[27] observed the orthorhombic–*I4/mcm* and *I4/mcm–Pm*$\bar{3}$*m* transitions in $CaTiO_3$ perovskite in their experiments, but for reasons unknown to us their transition temperatures are some 110 °C lower than observed here and by Kennedy *et al.*[16]

The linear variation of transition temperatures with composition (Fig. 6), extending (within experimental error) right to the $CaTiO_3$ end member, implies that a plateau effect, if any, is small. Plateau effects[28] originate from the lack of interaction of relaxation spheres around substituting atoms. It therefore appears that in the Sr for Ca substitution these spheres are large (or the lattice is stiff), whereas in defect perovskites such as those of the system $CaTiO_3$–$CaFeO_{2.5}$[29] local relaxation is aided by the presence of oxygen vacancies, and plateau effects are pronounced.

Finally, we have taken the transition temperature for the tetragonal to cubic transition reported by Hayward and Salje[30] to show (Fig. 6) the drop of the transition temperature towards lower values due to quantum saturation effects in compositions close to the $SrTiO_3$ end-member. At low temperatures, the behaviour of structural phase transitions is modified by the influence of quantum fluctuations. Such fluctuations enhance the stability of the high-symmetry phase, reducing the observed transition temperature (see ref. 31 and refs. therein). DSC measurements at low temperatures are planned to better define the phase boundary at these concentrations as well as to study the thermodynamics of the transition at these temperatures. Such measurements may then also shed light onto the additional phase transition reported by Ranjan and Pandey[14] at temperatures 25–30 K below the tetragonal to cubic transition in Sr-rich compositions, for which we see no evidence here.

Conclusions

The most likely sequence of phase transitions at room temperature in the perovskite system $Ca_{1-x}Sr_xTiO_3$ ($0 \leqslant x \leqslant 1$) and at high temperature for $Ca_{0.6}Sr_{0.4}TiO_3$ is:

$x=0.40$	$x \approx 0.45(5)$		$x \approx 0.65(5)$		$x \approx 0.92(2)$	
Pbnm	→	*Bmmb*	→	*I4/mcm*	→	*Pm*$\bar{3}$*m*
RT	375(25) °C		525(25) °C		800(50) °C	

The second orthorhombic phase (*Bmmb*) could not been determined in $Ca_{0.8}Sr_{0.2}TiO_3$ perovskite, either due to the poor resolution of the diffractometer employed in this case or because the *Bmmb* phase may not have a stability field at this composition. Transition temperatures for this composition are 875(25) °C for orthorhombic (*Pbnm* or *Bmmb*)–*I4/mcm* and 1100(50) °C for *I4/mcm–Pm*$\bar{3}$*m*.

In composition–temperature space, phase boundaries in $Ca_{1-x}Sr_xTiO_3$ perovskites shift linearly towards lower strontium content with the increase of temperature. At the $CaTiO_3$ end of the system the plateau effect is negligible or null whereas quantum saturation occurs near $SrTiO_3$.

Acknowledgements

The high temperature XRD experiments were performed in the Earth Sciences Laboratory, University of Cambridge and Department of Physics, Technical University of Denmark. H. Hillebrecht, Bayreuth, has been helpful in the acquisition of high-temperature DSC data at Netzsch and Linseis companies. QS acknowledges support by the scholarship of Universität Bayreuth, Germany and FS that by Fonds der Chemischen Industrie. This work has been supported in part by the EU through the TMR Network number ERB-FMRX-CT97-0108.

References

1 P. M. Woodward, *Acta Crystallogr., Sect. B*, 1997, **53**, 44.
2 J. S. Kim and S. J. L. Kang, *J. Am. Ceram. Soc.*, 1999, **82**, 119 and references therein.
3 A. E. Ringwood, S. E. Kesson, K. D. Reeve, D. M. Levins and E. J. Ramm, in *Radioactive Waste Forms for the future*, ed. W. Lutze and R. C. Ewing, North Holland Publishing, Amsterdam, 1987.
4 M. McQuarrie, *J. Am. Ceram. Soc.*, 1955, **38**, 444.
5 D. Kolar, M. Trontelj and Z. Stadler, *J. Am. Ceram. Soc.*, 1982, **40**, 373.
6 S. Sasaki, T. Prewitt and J. D. Bass, *Acta Crystallogr., Sect. C*, 1987, **43**, 1668.
7 R. H. Buttner and E. N. Maslen, *Acta Crystallogr., Sect. B*, 1992, **48**, 639.
8 H. Granicher and O. Jakits, *Suppl. Nuovo Cimento*, 1954, **9**, 580.
9 M. Mitsui and W. B. Westphal, *Phys. Rev.*, 1961, **124**, 1354.
10 M. Ceh, D. Kolar and L. Golic, *J. Solid State Chem.*, 1987, **68**, 68.
11 T. Hirata, K. Ishioka and M. Kitajima, *J. Solid State Chem.*, 1996, **124**, 353.
12 C. J. Ball, B. D. Begg, D. J. Cookson, G. J. Thorogood and E. R. Vance, *J. Solid State Chem.*, 1998, **139**, 238.
13 R. Ranjan, D. Pandey, V. Siruguri, P. S. R. Krishna and S. K. Paranjpe, *J. Phys.: Condens. Matter*, 1999, **11**, 2233.
14 R. Ranjan and D. Pandey, *J Phys.: Condens. Matter*, 1999, **11**, 2247.
15 S. A. T. Redfern, *J. Phys.: Condens. Matter*, 1996, **8**, 8267.
16 B. J. Kennedy, C. J. Howard and B. C. Chakoumakos, *J. Phys.: Condens. Matter*, 1999, **11**, 1479.
17 E. H. K. Salje, A. Graeme-Barber and M. A. Carpenter, *Acta Crystallogr., Sect. B*, 1993, **49**, 387.
18 A. C. Larson and R. B. Von Dreele, GSAS: General Structural Analysis System, LANSCE, Los Alamos National Laboratory, Los Alamos, NM, The Regents of the University of California, 1994.
19 R. A. Robie, B. S. Hemingway and J. R. Fisher, in *Thermodynamic properties of minerals and related substances at 298.5 K and 1 bar (10^5 Pascals) pressure and at higher temperatures*, US Government Printing Office, Washington, 1979, p. 456.
20 C. J. Howard and H. T. Stokes, *Acta Crystallogr., Sect. B*, 1998, **54**, 782.
21 A. M. Glazer, *Acta Crystallogr., Sect. B*, 1972, **28**, 3384.
22 R. M. Hazen, *Phys. Chem. Minerals*, 1977, **1**, 83.
23 M. Ahtee, A. AM. Glazer and A. W. Hewat, *Acta Crystallogr., Sect. B*, 1978, **34**, 752.
24 Y. Zhao and D. J. Weidner, *Phys. Chem. Minerals*, 1991, **18**, 294.
25 B. J. Kennedy, C. J. Howard and B. C. Chakoumakos, *Phy. Rev. B*, 1999, **59**, 4023.

26 X. Liu, Y. Wang, R. C. Liebermann, P. D. Maniar and A. Navrotsky, *Phys. Chem. Minerals*, 1991, **18**, 224.
27 F. Guyot, P. Richet, Ph. Courtial and Ph. Gillet, *Phys. Chem. Minerals*, 1993, **20**, 141.
28 E. H. K. Salje, *Eur. J. Mineral.*, 1995, **7**, 791.
29 A. I. Becerro, F. Seifert, R. J. Angel, S. Ríos and C. McCammon, *J. Phys.: Condens. Matter.*, 2000, **12**, 3661.
30 S. Hayward and E. K. H. Salje, *Phase Transit.*, 1999, **68**, 501.
31 S. Hayward and E. K. H. Salje, *J. Phys.: Condens. Matter.*, 1998, **10**, 1421.